Courant Number Independent Advection of the Moisture Quantities for the LMK

Jochen Förstner, Michael Baldauf and Axel Seifert

Deutscher Wetterdienst, Offenbach am Main, Germany

1 Introduction

The main part of the development of the two-timelevel dynamical core for the very short-range forecast model LMK was presented in the *COSMO Newsletter No. 4* (Förstner and Doms 2004; Doms and Förstner 2004). It follows closely the ideas of Wicker and Skamarock (2002) for the WRF model. The two most noteworthy differences are an option to use a truely third order Runge-Kutta scheme in the LMK, which is known in the literature (Liu et.al. 1994) as total variation diminishing (TVD) and, maybe more important, the formulation of the basic model equations. While in the WRF model the conservation form is used, in the LMK, which is based on the original LM code, we use the advection form. Idealized tests of the new dynamical core show good results (Baldauf et.al. 2005) and the TVD variant is used as default setting. While the integration of the dynamics is costly, we are able to use a bigger time step (30 s at 2.8 km) which leads in the end to a better efficiency than with the old Leapfrog core. Although the wind speed is restricted to 111 m/s, we have to deal with Courant numbers bigger than one — for the vertical this is the case anyway.

In the beginning of the LMK project stable integration of the prognostic equations for the moisture quantities (q_x) was realized by doing two sequential Eulerian advection steps with half the time step of the dynamics to ensure Courant numbers less than one. For the advection a positive definite but rather diffusive flux correction method with a monotonized-centered limiter was used.
To be able to do the advection of q_x in a single step, different methods for Courant number independent (CRI) transport have been implemented. Semi-Lagrange advection of the precipitating quantities was realized for the operational Leapfrog version. To retain positive definiteness (PD) of the scheme only tri-linear interpolation is used. While this leads to extreme numerical diffusion this might not be a problem for the precipitating fields. But for water vapor, cloud water and cloud ice this is not sufficient. Therefore in the combination with the Runge-Kutta core tri-cubic interpolation is used for these quantities, but the higher order is payed with the loss of PD.

It is also possible to construct CRI versions Eulerian schemes in flux-form and the way to do this is described. As an alternative to the semi-Lagrangian transport, in this paper we present a CRI version of Bott's advection scheme which has the advantage of being PD.

With respect to the quantitative precipitation forecast a new way to couple microphysics and dynamics, which is described in the latest WRF documentation (Skamarock et.al. 2005a), was recently implemented for the LMK and seems to be quite promising so far. This new variant is discussed briefly and first results are shown below.

2 Splitting, Conservation and Courant Number Independent Eulerian Advection

Skamarock (2005b) summarizes and presents ideas which combine several desirable properties of transport schemes used up to day. He concentrates on Eulerian schemes in flux-form

and addresses splitting errors, mass conservation, Courant number restriction and positive definiteness or even monotonicity. To reduce the splitting error associated with multidimensionality we use the Strang-splitting technique

$$q_x^{t+\Delta t} = (I + A_z)(I + A_y)(I + A_x)\; q_x^t \tag{1}$$

$$q_x^{t+2\Delta t} = (I + A_x)(I + A_y)(I + A_z)\; q_x^{t+\Delta t} \tag{2}$$

as a good and cheap compromise, where the sequence of the Marchuk-splitting of the different directions is reversed for each new time step. Here I is the identity operator and the A's are the advection operators in the different spatial directions.

Since the model equations of LM/LMK are formulated in advection form

$$\frac{\partial q_x}{\partial t} + \vec{v} \cdot \nabla q_x = \ldots, \tag{3}$$

we have to deal with the problem that the schemes in mind compute the divergence of the flux. Different options to do this are implemented. The first ("Flux Form - DIV") is to subtract the missing term which includes the 3D wind divergence

$$\frac{\partial q_x}{\partial t} + \nabla \cdot (\vec{v} q_x) - q_x \nabla \cdot \vec{v} = \ldots, \tag{4}$$

the second is to switch to the "Conservation Form"

$$\frac{\partial \rho q_x}{\partial t} + \nabla \cdot (\rho \vec{v} q_x) = \ldots \tag{5}$$

for the moisture transport by multiplying the specific values with the air density:

$$\rho_x^{(n)} = \rho^{(n)} q_x^{(n)}. \tag{6}$$

Afterwards the resulting moisture densities are transported

$$\begin{aligned} \rho_x^{(*)} &= \rho_x^{(n)} \;\; + \Delta t \; A_x\big(\rho_x^{(n)}\big) \\ \rho_x^{(**)} &= \rho_x^{(*)} \;\; + \Delta t \; A_y\big(\rho_x^{(*)}\big) \\ \rho_x^{(n_{adv})} &= \rho_x^{(**)} + \Delta t \; A_z\big(\rho_x^{(**)}\big) \end{aligned} \tag{7}$$

and in the end we have to transform them back to the specific values

$$q_x^{(n+1)} = \frac{\rho_x^{(n_{adv})}}{\rho^{(n_{adv})}}. \tag{8}$$

To do this we need the updated $\rho^{(n_{adv})}$ and two different variants for its calculation are implemented in the LMK. Either to use the following diagnostic relation based on the equation of state:

$$\rho^{(n_{adv})} = \frac{p_0 + p^{*(n+1)}}{R_d T^{(n+1)}} - \left(\left(\frac{R_v}{R_d} - 1 \right) \rho_v^{(n_{adv})} - \rho_c^{(n_{adv})} - \rho_s^{(n_{adv})} \right) \tag{9}$$

where we use the updated $\rho^{(n_{adv})}$ in the remaining calculations of the time step. Or to do a prognostic calculation of the continuity equation

$$\begin{aligned} \rho^{(*)} &= \rho^{(n)} \;\; + \Delta t \; A_x\big(\rho^{(n)}\big) \\ \rho^{(**)} &= \rho^{(*)} \;\; + \Delta t \; A_y\big(\rho^{(*)}\big) \\ \rho^{(n_{adv})} &= \rho^{(**)} + \Delta t \; A_z\big(\rho^{(**)}\big) \end{aligned} \tag{10}$$

where the air density is advected in the same way as the moisture densities (7). In this case $\rho^{(n_{adv})}$ is used for (8) only, afterwards we continue to use $\rho^{(n)}$.

Our results so far showed that the prognostic variant (10) is to be preferred and all simulations shown below for which the conservation form was used are done in this way.

The basic idea to remove the Courant number restriction of advection schemes which use forward-in-time differencing is described, e.g. by Lin and Rood (1996). During the calculation, the fluxes at the cell interfaces are split into their integer (12) and fractional (13) part

$$Cr_{j+\frac{1}{2}} = u_{j+\frac{1}{2}} \frac{\Delta t}{\Delta x} \tag{11}$$

$$K_{j+\frac{1}{2}} = \mathrm{INT}(Cr_{j+\frac{1}{2}}) \tag{12}$$

$$Cr'_{j+\frac{1}{2}} = \mathrm{MOD}(Cr_{j+\frac{1}{2}}, K_{j+\frac{1}{2}}) \tag{13}$$

and only the fractional part is treated by a standard flux-form advection scheme which is restricted to $Cr \leq 1$:

$$f'_{j+\frac{1}{2}} = f'\left(Cr'_{j+\frac{1}{2}}, j - K_{j+\frac{1}{2}}\right) \tag{14}$$

$$\frac{\Delta t}{\Delta x} F_{j+\frac{1}{2}} = \begin{cases} \sum_{k=1}^{K_{j+\frac{1}{2}}} \rho_{x\,j-k+1}, & K_{j+\frac{1}{2}} \geq 1 \\ 0, & K_{j+\frac{1}{2}} = 0 \\ \sum_{k=-1}^{K_{j+\frac{1}{2}}} \rho_{x\,j-k}, & K_{j+\frac{1}{2}} \leq -1. \end{cases} \tag{15}$$

The total flux at a cell boundary is then given as the sum of the integer flux $F_{j+\frac{1}{2}}$ (15) and the fractional flux $f'_{j+\frac{1}{2}}$ (14).

3 CRI Version of Bott's Positive Definite Advection Scheme

Several Eulerian flux-form advection schemes are now implemented in a CRI way in the LMK, i.e. for the calculation of the fractional flux (14): First a van Leer-type scheme with a monotonized centered flux limiter (van Leer 1977), second the PPM scheme (with no flux limitation) used in Skamarock (2005b) — while the former is even monotone, it is also rather diffusive, whereas the latter is indeed less diffusive, but lacks the property of being positive definite. Therefore, as a third scheme with low numerical diffusion, we concentrate on the positive definite version of Bott's (1989a, 1989b) integrated flux form method.

The Bott scheme is realized in two variants with either second or fourth order polynomials and the procedure starts with the calculation of the integrated (fractional) fluxes given by

$$I^{+}_{j+\frac{1}{2}} = \sum_{k=0}^{l=2/4} \frac{\alpha_{j-K_{j+\frac{1}{2}},k}}{(k+1)2^{k+1}} \left[1 - \left(1 - 2Cr'^{+}_{j+\frac{1}{2}}\right)^{k+1}\right] \tag{16}$$

$$I^{-}_{j+\frac{1}{2}} = \sum_{k=0}^{l=2/4} \frac{\alpha_{j+1-K_{j+\frac{1}{2}},k}}{(k+1)2^{k+1}} \left[1 - \left(1 + 2Cr'^{-}_{j+\frac{1}{2}}\right)^{k+1}\right](-1)^k \tag{17}$$

$$I_j = \sum_{k=0}^{l=2/4} \frac{\alpha_{j-K_{j+\frac{1}{2}},k}}{(k+1)2^{k+1}} \left[(-1)^k + 1\right] \tag{18}$$

where the $\alpha_{j,k}$ are the mentioned polynomials of order l which are listed in Bott (1989b, Table 1). Equation (16) is the flux for positive $Cr\,'$, (17) is the flux for negative $Cr\,'$ and (18) is the flux corresponding to $Cr = 1.0$ which is used for normalization.

Applying the following constraints for positive definiteness of the scheme

$$i^+_{j+\frac{1}{2}} = \max\left(0, I^+_{j+\frac{1}{2}}\right) \tag{19}$$

$$i^-_{j+\frac{1}{2}} = \max\left(0, I^-_{j+\frac{1}{2}}\right) \tag{20}$$

$$i_j = \max\left(I_j, i^+_{j+\frac{1}{2}} + i^-_{j-\frac{1}{2}} + \epsilon\right) \tag{21}$$

the fractional flux at a cell boundary is finally given by

$$f'_{j+\frac{1}{2}} = \frac{\Delta x}{\Delta t}\left[\frac{i^+_{j+\frac{1}{2}}}{i_j}\psi_{j-K_{j+\frac{1}{2}}} - \frac{i^-_{j+\frac{1}{2}}}{i_{j+1}}\psi_{j+1-K_{j+\frac{1}{2}}}\right]. \tag{22}$$

When we compare the CPU time for a real case simulation, where advection is calculated for all six prognostic moisture variables q_v, q_c, q_i, q_r, q_s and q_g, while the fourth order version is slightly more expensive, the second order one is comparable to the semi-Lagrangian transport in this respect. All in all with the CRI version of the Bott scheme we get a high order positive definite scheme at a reasonable computational cost.

4 Tri-cubic Semi-Lagrange Advection

A Semi-Lagrange (SL) scheme for the advection equation (3) is usually performed in two steps: first in estimating the point, from where a fluid particle started at the beginning of the time step, i.e. in calculating a backtrajectory and second in interpolating properties at the starting point from the neighboring grid points (Staniforth and Coté 1991).

The backtrajectory of 2^{nd} order is calculated as described in Baldauf and Schulz (2004). The result is a shift vector of the starting point relative to the actual grid point. The integer part of this shift vector delivers the grid position of the interpolation polynomial and the fractional part delivers the interpolation weights (for consistency with the tri-linear SL-routine these weights lie between -1 and 0). Therefore the following interpolation takes place in the transformed (or index) space.

For the tri-cubic interpolation a polynomial $p(x, y, z)$ is searched with the property $p(i, j, k) = q_{i,j,k}$, where i, j, $k = -2, -1, 0, 1$, and $q_{i,j,k}$ is the value at the appropriate grid point. This problem can be reduced to the estimation of polynomials $P_k(x)$ of only one variable x with the property

$$P_i(j) = \begin{cases} 1 & : \quad i = j \\ 0 & : \quad i \neq j \end{cases}, \qquad i, j = -2, -1, 0, 1, \tag{23}$$

which is fulfilled by

$$P_{-2}(x) = \frac{1}{6}\,(x+1)\,x\,(x-1), \tag{24}$$

$$P_{-1}(x) = -\frac{1}{2}\,(x+2)\,x\,(x-1), \tag{25}$$

$$P_0(x) = \frac{1}{2}\,(x+2)\,(x+1)\,(x-1), \tag{26}$$

$$P_1(x) \;=\; -\frac{1}{6}\,(x+2)\,(x+1)\,x. \tag{27}$$

The polynomial p can then be constructed by

$$p(x,y,z) = \sum_{i,j,k=-2}^{1} P_i(x)\; P_j(y)\; P_k(z)\; q_{i,j,k}, \tag{28}$$

where x, y, z are the interpolation weights. The sum (28) runs over the neighboring 64 grid points of the backtrajectory starting point. These are much more points than are needed to construct a polynomial of only 3^{rd} order in 3 dimensions; for this task only 20 grid points would be necessary. But the high symmetry of equation (28) allows a quick way for calculating the sum. Therefore this SL variant is rather efficient and nevertheless possesses rather good transport properties. Another advantage of this SL-method is, that it calculates the interpolation in three dimensions in one step, therefore no splitting error occurs. However a disadvantage is, that the method can produce negative undershoots for a positive definite field. Clipping of these negative values can destroy the rather good conservation properties of this SL-method. To reduce sharp edges, which can produce stronger undershoots, a smoothing filter is applied before clipping.

5 New Physics-Dynamics-Coupling

A special procedure to couple microphysics and dynamics is described in the latest WRF documentation (Skamarock et.al. 2005a). A similar numerical treatment of latent heat is now implemented in the Runge-Kutta core of the LMK. In both models the microphysic parameterization is calculated in one Eulerian time step after the Runge-Kutta integration of the dynamical core and the Marchuk-splitting method is used here to finally update the fields in a balanced way and complete the time step.

The diabatic heating term in the prognostic equation for temperature Q_T in the LM(K) includes the physical tendencies due to radiation, convection, turbulent mixing and latent heat conversion in the microphysics (e.g. the saturation adjustment). While the former tendencies are integrated within the acoustic steps the last temperature tendency has not been part of this integration.

The new variant now uses the tendency due to latent heat conversion of the previous time step as an estimate which enters the integration of the fast waves in the same way than the other physical tendencies. After the Runge-Kutta update, this tendency estimate is subtracted again and the time step is completed as before.

6 Idealized Advection Tests

To verify the correct implementation and for comparison of the different schemes idealized advection tests were carried out with the LMK.
As a first and also very common test, the solid body rotation of a tracer cone was simulated (Fig. 1). In the case shown, the angular velocity was rather high, leading to Courant Numbers well above one.
All of the four schemes perform equally well, at least in two aspects: First the Courant number independence is fulfilled, since in each case we get a stable integration. Second the circular shape of the cone is more or less retained, i.e. errors due to the directional splitting method used for the Bott scheme are negligible. For a further investigation of this last property idealized tests utilizing a deformational flow field are planned.

The Bott scheme using 4^{th} order polynomials (Fig. 1(c)) performs best. It is positive definite (up to an ε) and the maximum value is retained well, that is the scheme shows only weak numerical diffusion. For the 2^{nd} order Bott scheme (Fig. 1(a)) we get a similar result with an only slightly smaller maximum, which is almost equal to the one we get for semi-Lagrangian variant using tri-cubic interpolation (Fig. 1(b)). But the higher order interpolation in this case leads to negative undershoots, i.e. the loss of positive definiteness of the scheme. While this does not happen when tri-linear interpolation (Fig. 1(d)) is used, the numerical diffusion of this scheme is extremely large and perhaps comparable to a 1^{st} order upwind scheme.

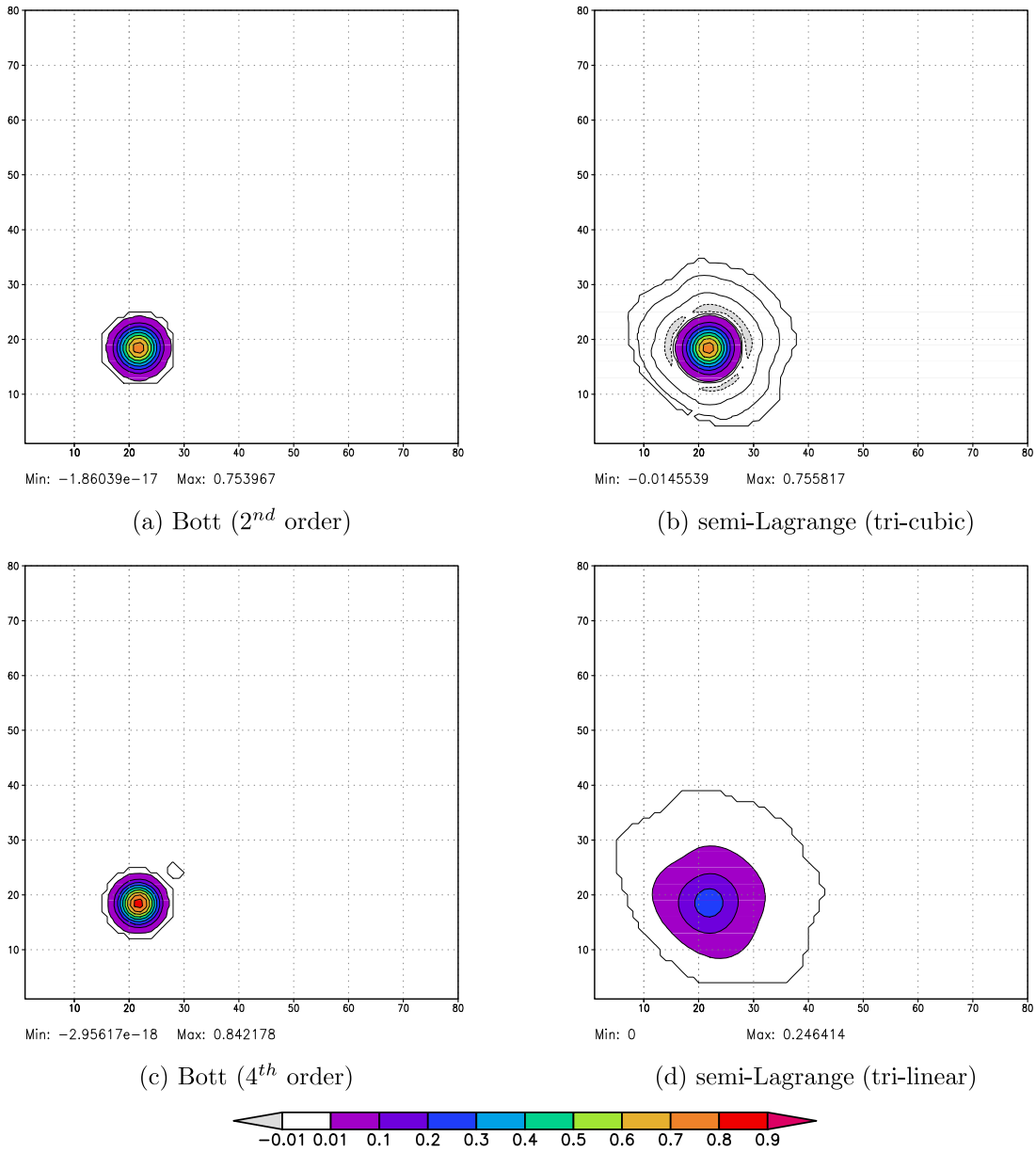

(a) Bott (2^{nd} order)

(b) semi-Lagrange (tri-cubic)

(c) Bott (4^{th} order)

(d) semi-Lagrange (tri-linear)

Figure 1: Solid body rotation of a tracer cone with an initial maximum of 1.0. Results after 80 time steps equivalent to one revolution. The Courant Number in the domain is close to a value of three near the lateral boundaries and approximately a value of 2.2 at the center of the cone.

From now on we will concentrate on two schemes, namely the Bott scheme formulated with the 2^{nd} order polynomials and the semi-Lagrangian scheme using the tri-cubic interpolation

to calculate the values at the starting point of the backtrajectory.

In a second test the tracer cone is advected in x- and z-direction (Fig. 2). The 35 layers used are stretched in the vertical as it was done in the once operational 7 km version of LM. This is a good test of the metrics in such a configuration.
The statements made for the solid body rotation test apply here in an analogous way. The increasingly ellipsoidal shape as the tracer cone is advected downwards is a drawing artefact. A real problem with the directional splitting would give rise to a tilted structure.

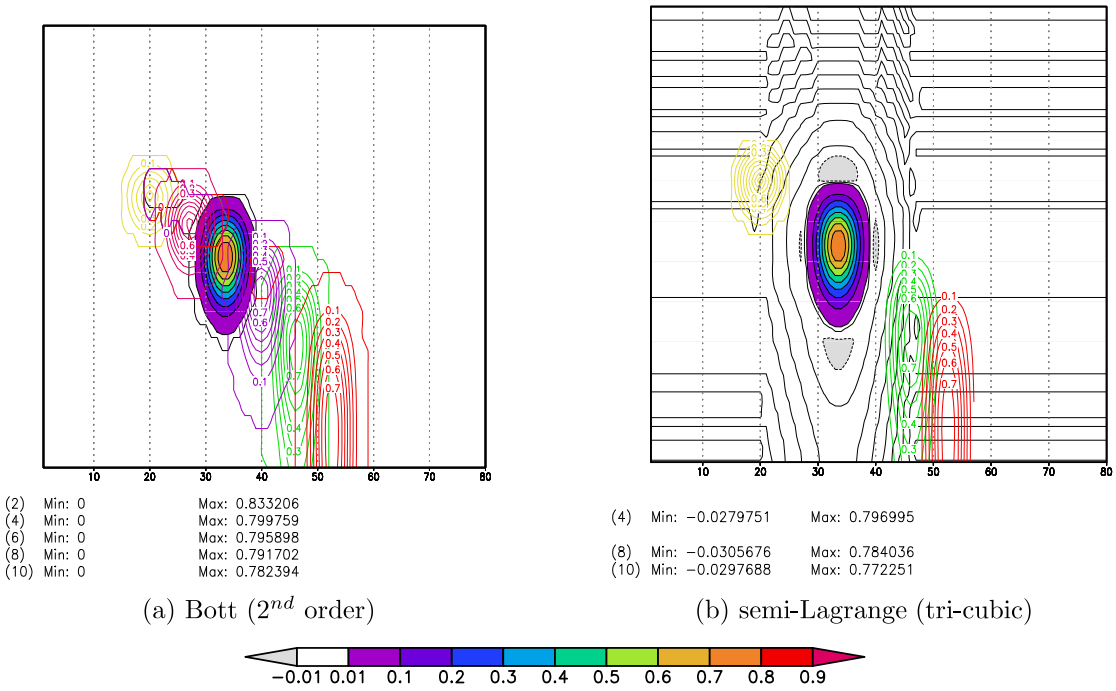

(a) Bott (2^{nd} order) (b) semi-Lagrange (tri-cubic)

Figure 2: xz-Advection with $u = 150$m/s and $w = -10$m/s of a tracer cone with an initial maximum of 1.0. Simulation times in minutes are given in parentheses. A vertically stretched grid is used which leads to values of $Cr_z = w\frac{\Delta t}{\Delta z}$ exceeding one near the bottom boundary. (The vertically stretched grid is not taken into account when directly plotting the model layers in GrADS.)

7 Real Case Studies

In real case studies we experience a big sensitivity of the model with respect to the different choices for moisture advection and the way in which we couple dynamics and the microphysic parameterization. As two examples Fig. 3 and Fig. 4 show a comparison of the 24 h precipitation over Germany for different advection schemes and observations. The data for each plot is aggregated to the LM grid with a resolution of 7 km.
The results differ significantly in the mean, their maximum and the precipitation pattern itself – especially when we look at the Southern border of Germany. The 24 h precipitation shows us to a certain degree the "integrated" performance of the model.
But the problems start when we look at the given observational data (Figs. 3(a) and 3(b), respectively 4(a) and 4(b)). The uncorrected radar data show obvious erroneous high values, e.g. in the vicinity of the radar sites, but very low values for the overall precipitation mean. Therefore we take the quality controlled data of the high-density rain-gauge observation network as the "truth".

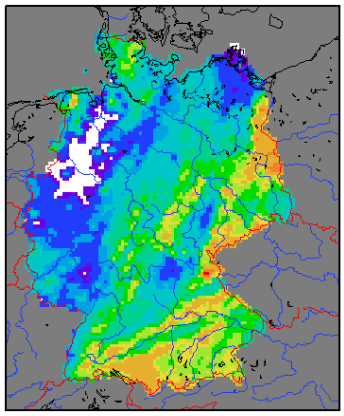

(a) High-Density Rain-Gauge Observation (= "truth")
Mean: 12.62 mm Max.: 90.16 mm

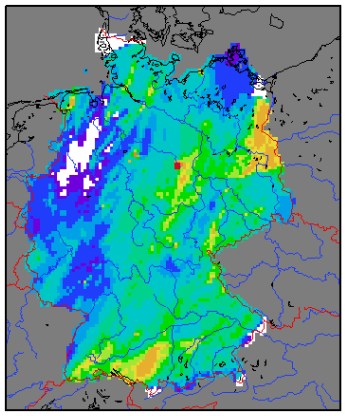

(b) Radar Observation (uncorrected)
Mean: 9.51 mm Max.: 120.47 mm

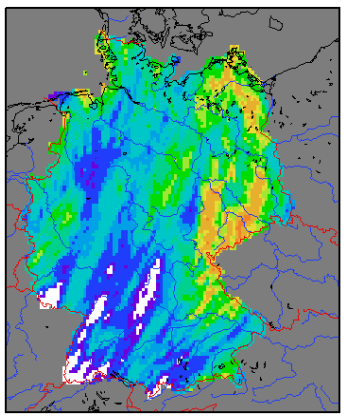

(c) Old Physics-Dynamics-Coupling: Bott (2^{nd} order) in Flux Form - DIV
Mean: 10.51 mm Max.: 69.79 mm

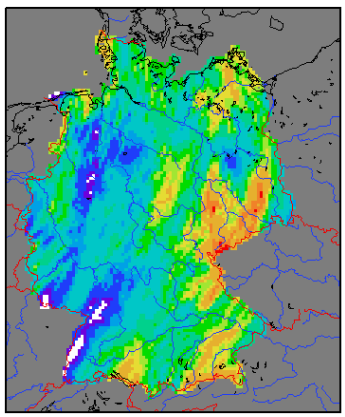

(d) Old Physics-Dynamics-Coupling: semi-Lagrange
Mean: 11.84 mm Max.: 87.48 mm

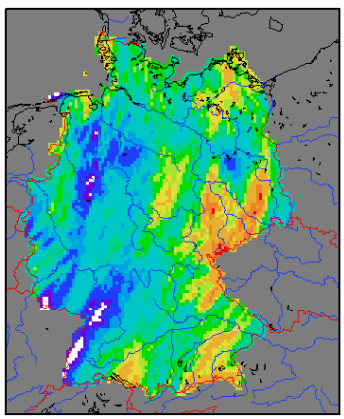

(e) New Physics-Dynamics-Coupling: Bott (2^{nd} order) in Conservation Form
Mean: 14.62 mm Max.: 94.56 mm

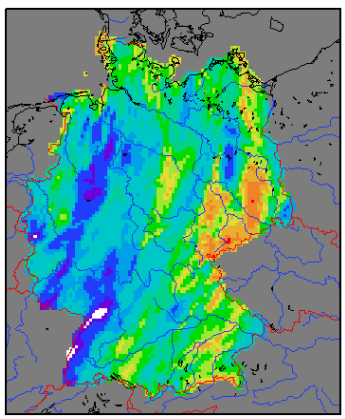

(f) New Physics-Dynamics-Coupling: semi-Lagrange
Mean: 13.19 mm Max.: 88.48 mm

Figure 3: Precipitation 07/08/2004 – 6:00 UTC + 24 h (Figures by Thorsten Reinhardt).

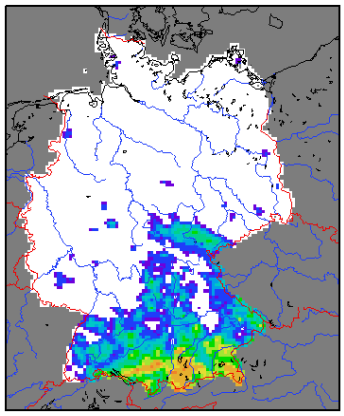

(a) High-Density Rain-Gauge Observation (= "truth")
Mean: 2.54 mm Max.: 63.60 mm

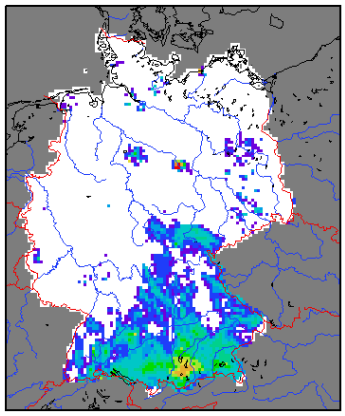

(b) Radar Observation (uncorrected)
Mean: 1.63 mm Max.: 139.28 mm

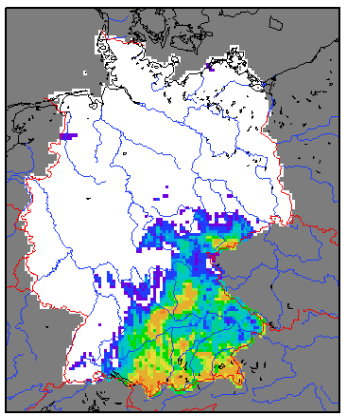

(c) Old Physics-Dynamics-Coupling: Bott (2^{nd} order) in Flux Form - DIV
Mean: 3.72 mm Max.: 61.04 mm

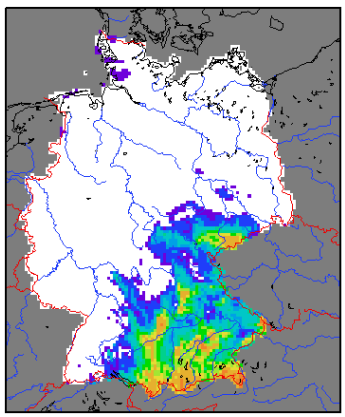

(d) Old Physics-Dynamics-Coupling: semi-Lagrange
Mean: 4.30 mm Max.: 138.36 mm

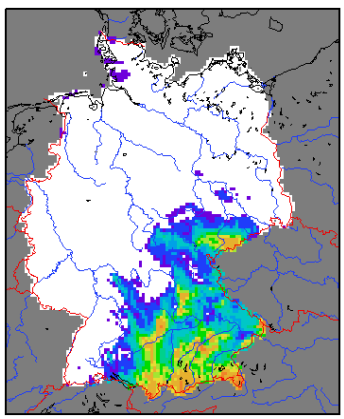

(e) New Physics-Dynamics-Coupling: Bott (2^{nd} order) in Conservation Form
Mean: 3.54 mm Max.: 77.23 mm

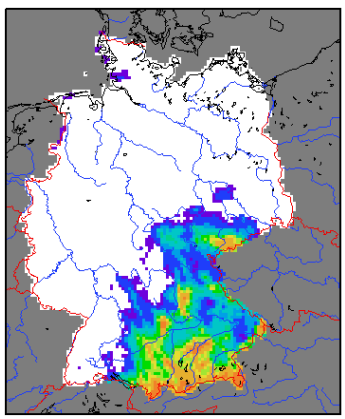

(f) New Physics-Dynamics-Coupling: semi-Lagrange
Mean: 3.77 mm Max.: 74.92 mm

Figure 4: Precipitation 07/24/2004 – 6:00 UTC + 24 h (Figures by Thorsten Reinhardt).

For both cases the two plots in the middle row show results obtained with the old coupling, whereas the plots in the bottom row were obtained using the new coupling.

For the semi-Lagrangian runs this is the only change, but in the runs with Bott's Eulerian scheme a second change was made, namely a switch from the non-conservative flux-form (4) to the conservation form (5).

Most noteworthy when we look at the results for the 07/08/2004 (Fig. 3) is the difference between Fig. 3(c) and Fig. 3(e) at the Southern border of Germany. In the run using the non-conservation form we get too little precipitation compared to the rain-gauge observation. This is probably due to the fact, that the term $-q_x \nabla \cdot \vec{v}$ in (4) which is only calculated in 2^{nd} order has a great potential to deteriorate the conservation of the specific moisture quantities. This problem will be addressed in more detail in the next section.
For the two different semi-Lagrangian runs (Fig. 3(d) and Fig. 3(f)) it is not obvious which variant of coupling gives us the better result — at least in this case.

When we look at the results for the 24/07/2004 (Fig. 4) it is somehow the other way round. Now the results for the Bott scheme (Fig. 4(c) and Fig. 4(e)) are more similar to each other, while the runs with the semi-Lagrange scheme (Fig. 4(d) and Fig. 4(f)) differ significantly in their maximum values of precipitation near and in the alpine region.

But for both cases the newer variants (in the bottom row) are at least as good or remarkably better than the old ones. And, what is important, the results for the Bott scheme and the semi-Lagrange scheme are very similar now.

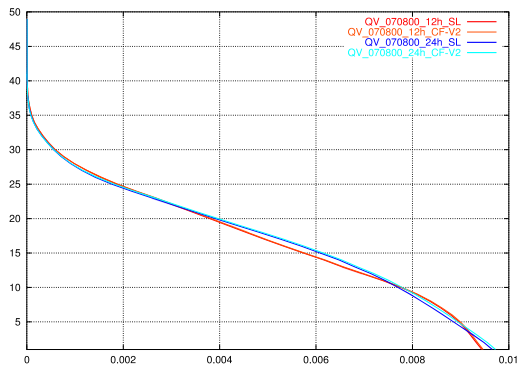

(a) q_v – 07/08/2004 00 UTC Run

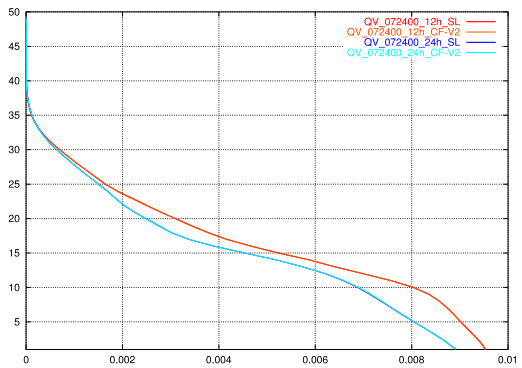

(b) q_v – 07/24/2004 00 UTC Run

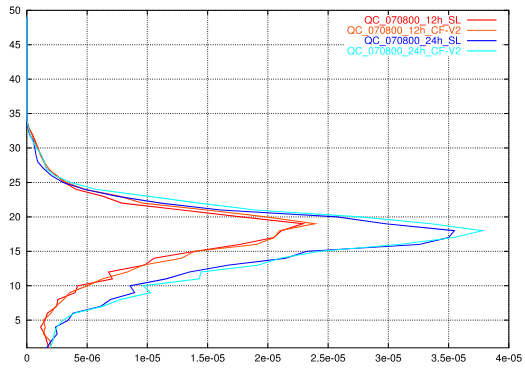

(c) q_c – 07/08/2004 00 UTC Run

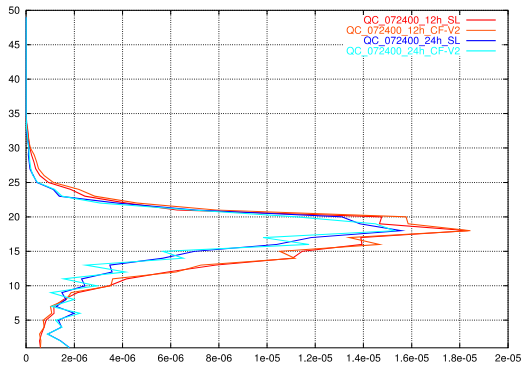

(d) q_c – 07/24/2004 00 UTC Run

Figure 5: Mean vertical profiles of specific water vapor and cloud water [kg/kg] for forecast times of 12 (red) and 24 (blue) hours.
lighter colors: Bott (2^{nd} order) in Conservation Form / darker colors: semi-Lagrange

This can also be seen in Fig. 5, where the domain averaged vertical profiles of water vapor and cloud water are plotted for both new variants and both dates (forecast times of 12 and 24 hours). Especially the profiles of water vapor lie almost on top of each other.
In the profiles of cloud water we notice a small scale zigzag-structure, most notably in the second case. The reason for this structure is not clear yet, but one explanation might be the rather poor quality of the only 2^{nd} order implicit vertical advection scheme for the wind components, pressure perturbation and temperature in the dynamical core. This low order centered scheme produces rather large undershoots and is also not free of numerical dispersion. Here, higher order schemes might have a big potential to further improve the model.

8 Tracer Experiment

The reasons for the differences we have seen, have to be investigated and discussed further, but they are at least partly a result of the varying numerical diffusivity and (missing) positive definiteness / mass conservation properties of the schemes.

Therefore a further experiment has been performed. In this experiment a tracer is transported in the flow field of the real case study for the date 07/08/2004 (00 UTC run) discussed in the previous section.
The tracer was initialized with a value equal to one, with the exception of a small cuboidal area in the middle of the domain (Fig. 6(a)). In this way we get a structure which is characterized by sharp gradients in an otherwise homogeneous field. In addition a zero-gradient lateral boundary condition was used for the tracer.
As long as the tracer structure remains inside the domain, the integral tracer mass should be conserved.

Figs. 6(b) to 6(d) show the tracer field after three hours of simulation time for different variants of advection. In each case, all moisture quantities were transported in the same way as the tracer, with the exception of q_r, q_s and q_g in the semi-Lagrangian case, for which the default tri-linear interpolation was used, i.e. the flow field differs from run to run for this reason. For all runs the new coupling of physics and dynamics was switched on and a clipping of negative tracer values was performed. This clipping acts as an artificial source if the overall advection scheme is not positive definite, and this is the case for all runs, with the only exception being the Bott scheme in conservation form (Fig. 6(c)) for which we get identical results for the runs with and without (not shown) clipping.

The result for the Bott scheme used in the non-conservative form given by Eq. (4) shows a tracer field with a lot of small scale disturbances over the whole domain. This pattern is due to the term including the 3D wind divergence, and a look at the divergence field (not shown here) shows similar small scale features especially pronounced over orographically structured terrain.
It is clear from this experiment, that it is probably not a good idea to use this form of advection, and it explains the deficiencies we have noticed in the precipitation pattern in the last section.

It was already stated that the conservative Bott scheme and the semi-Lagrangian scheme in the new form produce quite similar results. This is also true for the tracer field (Fig. 6(c) and 6(d)). A closer look shows some minor artifacts around level 39 in the plot for the Bott scheme. This is approximately the level where the Rayleigh damping layer begins, but a real explanation is still missing. It is also worth to notice, that in the homogeneous parts of the tracer field, the interpolation step in the semi-Lagrange scheme is quite trivial. On the other

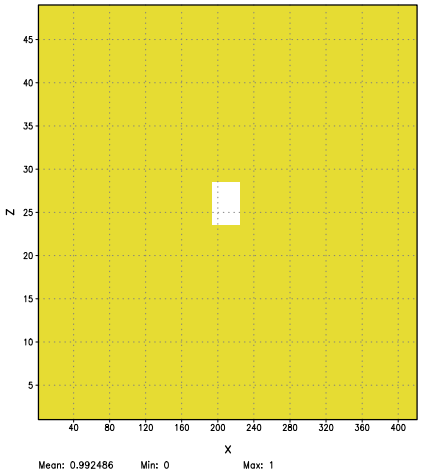

(a) Initialized tracer distribution at y-index $j = 230$ (middle of domain).

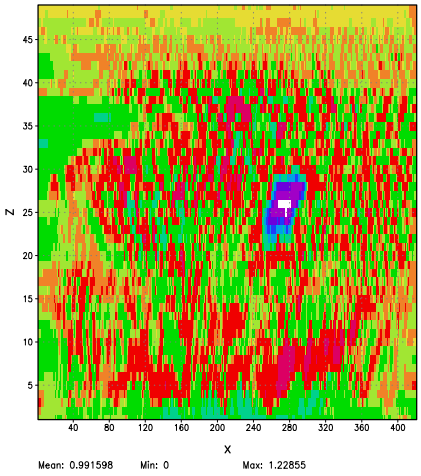

(b) Tracer distribution after 3 h at y-index $j = 260$ – Bott (2^{nd} order) in Flux Form - DIV with Clipping of Negative Values.

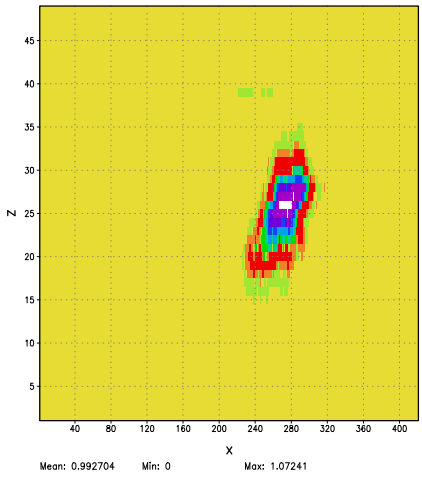

(c) as (b) – Bott (2^{nd} order) in Conservation Form.

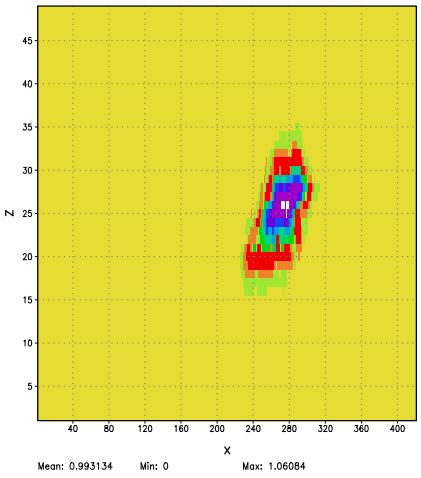

(d) as (b) – semi-Lagrange (tri-cubic) with Clipping of Negative Values.

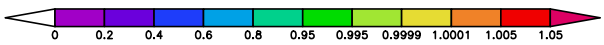

Figure 6: Advection of a tracer in a real case flow field (07/08/2004 00 UTC run). Shown are vertical cross sections of the tracer field. (The vertically stretched grid is not taken into account when directly plotting the model layers in GrADS.)

hand in the Bott scheme in conservation form, the mass specific tracer field is multiplied with the air density, and afterwards the resulting exponentially distributed tracer density has to be transported.

In Fig. 7 the normalized volume integral of the tracer field is given as time series over the first 360 steps. The red curve corresponds to the run given in Fig. 6(c), and the blue one corresponds to Fig. 6(d). In addition, shown in green is the result for a semi-Lagrangian run without the clipping of negative values. As stated in Sec. 4, the semi-Lagrange scheme with tri-cubic interpolation, for itself, has good conservation properties, and it follows closely the line of the conservative Bott scheme. But the clipping of undershoots — which arise near sharp gradients, to circumvent negative values, acts as an artificial source. As soon as this sharp gradients are diffused to a certain extend — in approximately the first 100 time steps

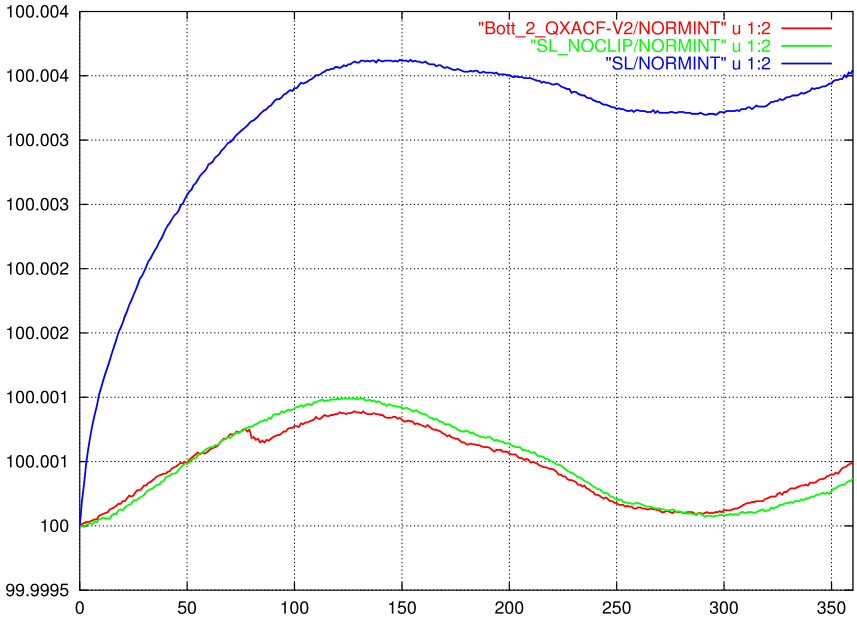

Figure 7: Time series of the normalized volume integral of the tracer field for the first three hours (360 time steps). The initialized value corresponds to 100 percent.
red: Bott (2^{nd} order) in Conservation Form / blue: semi-Lagrange (tri-cubic) with Clipping of Negative Values / green: semi-Lagrange (tri-cubic) without Clipping of Negative Values.

in this case, the curves for the runs with and without clipping stay more or less parallel.

9 Conclusions

The two different advection schemes, namely the semi-Lagrangian one and the Eulerian Bott scheme in conservation form, have been developed independently from each other. And the fact that they produce very similar results, at least in the cases investigated so far, makes us quite confident, with respect to their (finally?) correct implementation into the LMK. The most recent changes are not part of the official version 3.16 yet, but will come in the next release.
Both variants have their pros and cons — being positive definite or not, being a real 3D or only a split 1D scheme, as well as the question, if all quantities should be transported in the same way, or, as it is done in the semi-Lagrangian variant, to make a distinction between the precipitating and non-precipitating quantities.
Further tests, comparisons and verifications, especially for runs over longer periods, are on their way and will help us to decide, which one of the two schemes is to be preferred — if we see significant differences then.

10 References

Baldauf, M. and J.-P. Schulz (2004). Prognostic Precipitation in the Lokal Modell (LM) of DWD. *COSMO-Newsletter*, No. 4, 177–180. Deutscher Wetterdienst, Offenbach a. M., Germany. availabe at `http://www.cosmo-model.org`.

Baldauf, M., J. Förstner, and P. Prohl (2005). Idealized Tests of the Very Short-Range Forecast Model LMK. *WGNE Blue Book*, `http://www.cmc.ec.gc.ca/rpn/wgne/`.

Bott, A. (1989a). A positive definite advection scheme obtained by nonlinear renormalization of the advective fluxes. *Mon. Wea. Rev.*, 117, 1006–1015.

Bott, A. (1989b). Reply. *Mon. Wea. Rev.*, 117, 2633–2636.

Doms, G. and J. Förstner (2004). Development of a kilometer-scale NWP-system: LMK. *COSMO Newsletter*, No. 4, 159–167. Deutscher Wetterdienst, Offenbach a. M., Germany. availabe at `http://www.cosmo-model.org`.

Förstner, J. and G. Doms (2004). Runge-Kutta Time Integration and High-Order Spatial Discretization of Advection – A New Dynamical Core for the LMK. *COSMO Newsletter*, No. 4, 168–176. Deutscher Wetterdienst, Offenbach a. M., Germany. availabe at `http://www.cosmo-model.org`.

Lin, S. J. and R. B. Rood (1996). Multidimensional flux-form semi-Lagrangian transport schemes. *Mon. Wea. Rev.*, 124, 2046–2070.

Liu, X.-D., S. Osher and T. Chan (1994). Weighted essentially non-oscillatory schemes. *J. Comput. Phys.*, 115, 200–212.

Skamarock, W. C., J. B. Klemp, J. Dudhia, D. O. Gill, D. M. Barker, W. Wang and J. G. Powers (2005a). A Description of the Advanced Research WRF Version 2. *NCAR Technical Note*, `http://www.wrf-model.org/wrfadmin/docs/arw_v2.pdf`. Boulder, Colorado, USA: Mesoscale and Microscale Meteorology Division NCAR.

Skamarock, W. C. (2005b). Positive-definite and montonic limiters for unrestricted-timestep transport schemes. accepted for *Mon. Wea. Rev.*,

Staniforth, A. and J. Coté (1991). Semi-Lagrangian integration schemes for atmospheric models — A review. *Mon. Wea. Rev.*, 119, 2206–2223.

van Leer, B. (1977). Towards the ultimate conservative difference scheme IV. A new approach to numerical convection. *J. Comp. Phys.*, 23, 276–299.

Wicker, L. J. and W. C. Skamarock (2002). Time-splitting methods for elastic models using forward time schemes. *Mon. Wea. Rev.*, 130, 2088–2097.